Earthquake Engineering & Structural Dynamics
The Journal of the International Association for Earthquake Engineering

EARTHQUAKE ENGINEERING & STRUCTURAL DYNAMICS
Earthquake Engng Struct. Dyn. 2013; **42**:1749–1765
Published online 23 April 2013 in Wiley Online Library (wileyonlinelibrary.com). DOI: 10.1002/eqe.2296

Actuator dynamics compensation based on upper bound delay for real-time hybrid simulation

Bin Wu[1,*,†], Zhen Wang[1,2] and Oreste S. Bursi[2]

[1] *School of Civil Engineering, Harbin Institute of Technology, Haihe Road, No. 202, Harbin 150090, China*
[2] *Department of Mechanical and Structural Engineering, University of Trento, Via Mesiano 77, Trento 38123, Italy*

SUMMARY

Real-time hybrid simulation represents a powerful technique capable of evaluating the structural dynamic performance by combining the physical simulation of a complex and rate-dependent portion of a structure with the numerical simulation of the remaining portion of the same structure. Initially, this paper shows how the stability of real-time hybrid simulation with time delay depends both on compensation techniques and on time integration methods. In particular, even when time delay is exactly known, some combinations of numerical integration and displacement prediction schemes may reduce the response stability with conventional compensation methods and lead to unconditional instability in the worst cases. Therefore, to deal with the inaccuracy of prediction and the uncertainty of delay estimation, a nearly exact compensation scheme is proposed, in which the displacement is compensated by means of an upper bound delay and the desired displacement is picked out by an optimal process. Finally, the advantages of the proposed scheme over conventional delay compensation techniques are shown through numerical simulation and actual tests.

Received 8 March 2012; Revised 8 January 2013; Accepted 21 February 2013

KEY WORDS: real-time hybrid simulation; delay compensation; upper bound delay; overcompensation; optimal feedback

1. INTRODUCTION

1.1. Background and motivation

In the past two decades, much attention has been paid to real-time hybrid simulation (RHS), as a novel technique able to evaluate the dynamic response of a structure [1–5]. In detail in RHS, the structure is divided into a physical substructure (PS) and a numerical substructure (NS), respectively; the coupling between the two parts is being handled by one or more numerical coordinators and physical transfer systems, for example, actuators. Therefore, synchronization at the interface is extremely important for accurate RHS. In this process, time delay is inevitable owing to the time spent during the computation performed by the numerical coordinator and to a large extent by the actuation of the physical transfer system. As a result, time delay reduces the response accuracy and in the worst case causes instability of RHS.

Most research efforts to reduce the negative effect of time delay have focused on the development of various compensation schemes for transfer systems. These schemes basically can be classified into two types: (i) to send the command in advance and (ii) to add a compensator with positive phase, that is, a lead compensator. In a hybrid simulation, the command sent to the PS is actually the calculated

*Correspondence to: Bin Wu, School of Civil Engineering, Harbin Institute of Technology, Haihe Road, No. 202, Harbin 150090, China.
†E-mail: bin.wu@hit.edu.cn

response at the interface between PS and NS; therefore, it cannot be known *a priori*. As a result, a response prediction is needed for the first type of compensation scheme. All available prediction methods are based on polynomial extrapolations, among which the third-order Lagrange polynomial proposed by Horiuchi and Konno for RHS is most widely applied [6]. Extrapolations based both on constant and linear variation of acceleration were also applied; mathematically, they can be classified as osculating polynomials, among which Lagrange and Hermite polynomials are two special cases [7]. The effect of time delay can also be compensated for by force correction, on the basis of polynomial curve fitting of measured data [8].

The ideal candidate among lead compensators is the compensator with adverse dynamics of the transfer system, while feedforward and phase lead are more widely used in mechanical control [9]. To cope with the problems of noise sensitivity and uncertainty modeling, low-pass filter and feedback control are combined with inverse dynamics [10, 11]. In this respect, Christenson *et al.* [12] suggested a virtual coupling; in greater detail, the effect of a virtual coupling is essentially equivalent to a first-order phase lead compensator with magnitude less than one.

In both these two types of compensation schemes, compensation effects could be impaired by the assumption of fixed time delay or constant actuator dynamics because they vary during a test. As a result, several online procedures for delay estimation and adaptive mechanisms capable of correcting parameters associated with delay were proposed [8, 13–15]. Although these methods worked well for certain situations, stability, robustness, and parameter design of the corresponding adaptive laws represent significant issues that require further investigation.

1.2. Scope

A straightforward alternative to treat the uncertainty of delay estimation is the upper bound delay or delay overcompensation because it entails an equivalent positive damping on the whole emulated structure. To ensure dynamic stability, overcompensation was used by Wallace *et al.* [16] in their adaptive delay compensation. However, the accuracy of RHS with overcompensation was reduced because, as a result of overcompensation, the force fedback to the NS did not correspond to the desired displacement. However, we underline that a nearly exact compensation could be achieved if the force datum to be collected is not the one at the current time instant but the one corresponding to the desired displacement, which can be chosen among overcompensated displacement data. Along this line, we propose, in this paper, an upper bound delay compensation strategy for RHS that entails a nearly exact compensation.

The reminder of this paper is organized as follows. Section 2 analyses problems that result from conventional compensation methods, even when the time delay τ is exactly known. Then, Section 3 presents the basis of the nearly exact compensation method that relies on an upper bound delay τ_c and an optimal feedback technique. In Sections 4 and 5, respectively, we present numerical simulations and actual tests, to show the effectiveness of the proposed delay compensation strategy. Finally, conclusions are drawn and necessary developments are described in Section 6.

2. PROS AND CONS ON DELAY COMPENSATION TECHNIQUES FOR RHS

It was shown that time delay mainly due to actuator dynamics introduces negative damping into the emulated system, whereas delay compensation entails positive damping in the low-frequency range [17]. However, this conclusion is based on the assumption that the dynamic response computed for the NS is exact. Apparently, the evaluated displacement response is affected by amplitude change and period distortion, owing to the numerical time integration employed. Therefore, it is important to re-examine the effect of delay compensation also considering the influence of time integration algorithms. It is expected that different time integration methods combined with displacement response predictions will entail different compensation effects. In greater detail, we consider hereafter the following: (i) the time integration LSRT2 method suggested by Bursi *et al.* [5]; (ii) four response prediction schemes based on the second-order and third-order

DOI: 10.1002/eqe

Hermite extrapolations [7]; and (iii) both the explicit Newmark method and the linear acceleration method [8]. The analysis of the explicit Newmark integration method combined with a linear acceleration prediction is provided in Appendix 1.

With regard to the LSRT2 method, Bursi *et al*. proposed a two-stage Rosenbrock-based method to perform RHS, which becomes dissipative in the high-frequency range of the response via a proper choice of user-defined parameters [5]. It was named LSRT2 method because it is L-stable and real-time compatible; that is, at the beginning of each time step, the LSRT2 method does not require knowledge of the solution or its derivatives at the end of the time step. To apply the LSRT2 method, the system of equations of motion is written in the first-order form as

$$\dot{\mathbf{y}} = \mathbf{f}(\mathbf{y}, t) = \left\{ \begin{matrix} \dot{\mathbf{x}} \\ \mathbf{r}(\mathbf{x}, \dot{\mathbf{x}}, t) \end{matrix} \right\} \tag{1}$$

with

$$\mathbf{y} = \left\{ \begin{matrix} \mathbf{x} \\ \dot{\mathbf{x}} \end{matrix} \right\}, \tag{2}$$

where **x** defines the displacement vector. In greater detail, the LSRT2 method entails

$$\mathbf{k}_1 = [\mathbf{I} - \gamma \Delta t \mathbf{J}]^{-1} \mathbf{f}(\mathbf{y}_i, t_i)\Delta t, \qquad \mathbf{y}_{i+\alpha_{21}} = \mathbf{y}_i + \alpha_{21}\mathbf{k}_1, \tag{3}$$

$$\mathbf{k}_2 = [\mathbf{I} - \gamma \Delta t \mathbf{J}]^{-1} \left(\mathbf{f}\left(\mathbf{y}_{i+\alpha_{21}}, t_{i+\alpha_2}\right) + \gamma_{21}\mathbf{J}\mathbf{k}_1\right)\Delta t, \qquad y_{i+1} = \mathbf{y}_i + b_1\mathbf{k}_1 + b_2\mathbf{k}_2, \tag{4}$$

where Δt is the time integration interval, **J** is the Jacobian operator, and the recommended algorithmic parameters read

$$\gamma = 1 - \frac{\sqrt{2}}{2}, \quad \alpha_2 = \alpha_{21} = 1/2, \quad \gamma_{21} = -\gamma, \quad b_1 = 0, \quad b_2 = 1. \tag{5}$$

While the displacement predictions relevant to both the explicit Newmark method and the linear acceleration method can be found in [8], the second-order and the third-order Hermite extrapolations are given by

$$x(t_{i+1} + \tau_c)' = \left(1 - \eta^2\right)x_{i+1} + \eta^2 x_i + \left(\eta + \eta^2\right)\Delta t' \dot{x}_{i+1} \tag{6}$$

$$x(t_{i+1} + \tau_c)' = \left(1 - 3\eta^2 - 2\eta^3\right)x_{i+1} + \left(3\eta^2 + 2\eta^3\right)x_i + \left(\eta + 2\eta^2 + \eta^3\right)\Delta t' \dot{x}_{i+1} + \left(\eta^2 + \eta^3\right)\Delta t' \dot{x}_i, \tag{7}$$

respectively, where $x(t_{i+1} + \tau_c)'$ denotes the predicted displacement at $(t_{i+1} + \tau_c)$; τ_c and $\Delta t'$ define the assumed upper bound time delay and time interval between two successive interpolation points, respectively; and η denotes the ratio of τ_c over $\Delta t'$. When the actual delay τ is known, $\tau_c = \tau$. The advantage of the Hermite extrapolation is that it can utilize the latest velocity information available from the LSRT2 method, and hence, a more accurate prediction is expected. If τ is precisely known, then the compensation effect depends mainly on the prediction accuracy.

If we assume that $\Delta t << \tau_c$ and the response of the NS is exact, then the prediction accuracy can be evaluated through a frequency domain analysis [8, 18]. As a result, the frequency response plots of the four different prediction methods are shown in Figure 1, with $\eta = 1$ and $\Omega' = \omega \Delta t'$, where ω denotes the signal circular frequency. The damping effect of the compensation process can be seen from the phase plot: a positive phase angle indicates positive damping and vice versa. Positive damping results for small Ω' with all prediction methods herein, which is similar to polynomial extrapolation [8]. For clarity, we define the stability margin $[\Omega']$ such that positive damping results for all $\Omega' \leq [\Omega']$,

DOI: 10.1002/eqe

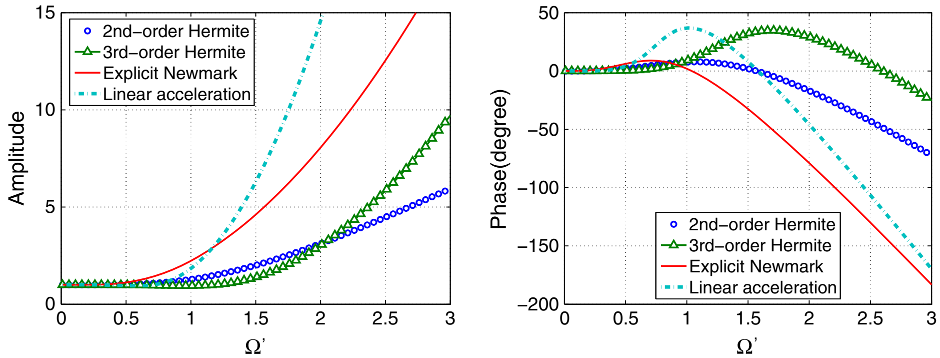

(a) Amplitude vs frequency (b) Phase vs frequency

Figure 1. Frequency response functions of various displacement prediction methods.

whereas negative damping is exhibited for $\Omega' > [\Omega']$. As a result, $[\Omega']$s read 1.58, 2.61, 1.05, and 1.59 for the second-order, third-order Hermite extrapolation, explicit Newmark, and linear acceleration methods, respectively.

To realistically evaluate the effectiveness of the aforementioned delay compensation schemes in an RHS, a spectral stability analysis was conducted on the undamped SDOF system shown in Figure 2. In the figure, k_e and k_n define the stiffness of PS and NS, respectively, and m_n is the assumed mass for the NS. When the equation of motion of the SDOF system is written in the Hamilton form, $\mathbf{f}(\mathbf{y},t)$ of Equation (1) is expressed as

$$\mathbf{f}(\mathbf{y},t) = \left\{ \begin{array}{c} \dot{x} \\ \left(-k_e x' - k_n x\right)/m_n \end{array} \right\}. \tag{8}$$

By means of Equations (3)–(8), the state vectors of the discretized system at successive time steps can be expressed as

$$\mathbf{X}_{i+1} = \mathbf{A}\mathbf{X}_i. \tag{9}$$

The state vector $\mathbf{X}_i$ and the corresponding amplification matrix $\mathbf{A}$ vary for different prediction methods. For instance for the third-order Hermite extrapolation techniques, $\mathbf{X}_i$ is defined as $\mathbf{X}_i = \left[x_{i-\frac{1}{2}} \quad \dot{x}_{i-\frac{1}{2}} \quad x_i \quad \dot{x}_i \quad x_i' \quad x_{i+\frac{1}{2}}' \right]^T$, where $x_{i-\frac{1}{2}}$ and $\dot{x}_{i-\frac{1}{2}}$ are structural responses at intermediate stages. The delay τ_c is assumed to be equal to the time integration interval Δt. Because the LSRT2 is a two-stage method, two predictions are carried out for each time step; that is, the prediction of x'_{i+1} is based on $\mathbf{y}_{i-\frac{1}{2}}$ and $\mathbf{y}_i$; $x'_{i+\frac{3}{2}}$ is based on $\mathbf{y}_i$ and $\mathbf{y}_{i+\frac{1}{2}}$.

The stability of the RHS can be evaluated by calculating the spectral radius of $\mathbf{A}$. In greater detail, Figure 3 shows the spectral radii of the LSRT2 method endowed with the aforementioned compensation schemes, where $\Omega = \sqrt{(k_n + k_e)/m_n}\Delta t$ and $k_n = k_e$. Note that we assumed that the

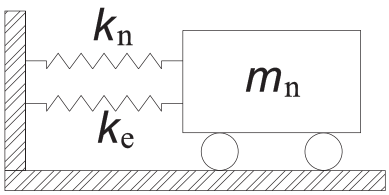

Figure 2. Computation model of an undamped SDOF system.

DOI: 10.1002/eqe

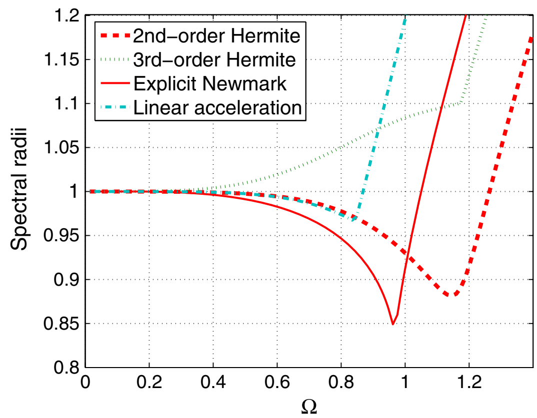

Figure 3. Stability of the RHS based on the LSRT2 method and different prediction methods.

dynamics of the transfer system is represented by a pure delay, which contrasts with the bilinear approximation of the step response assumed in [19]. From Figure 3, we can see that among the four compensation methods, the one based on the second-order Hermite extrapolation possesses the largest stable range for the LSRT2 method; it ranks third in Figure 1, when the time integration is not considered. It is more surprising to observe that the method based on the third-order Hermite extrapolation becomes unstable for small values of Ω, in contrast with its largest stability margin exhibited in Figure 1. These trends can be verified by means of a theoretical investigation on stability for small values of Ω and of a zero-stability analysis both presented in Appendix A2. Similar behavior can also be found for a delay compensation technique based on the more traditional explicit Newmark integration method with a linear acceleration prediction, as demonstrated in Appendix 1.

From the aforementioned analysis, we can see clearly that the stability of RHS characterized by time delay is not only related to compensation methods but also to integration methods; a better prediction accuracy provided by a frequency response of the prediction itself does not indicate a better performance of RHS. In other words, the stability of the time integration method is affected by the inaccuracy of prediction employed for delay compensation; this interaction is quite complex. Moreover, the delay τ_c is assumed to be constant and known in the analysis, whereas in actual tests, τ may vary because of changes in the specimen stiffness, reaction force, and signal frequency. The aforementioned analysis also assumed that the transfer system or actuator could simply be modeled as a dead time, and hence, no amplitude control error existed. Actual transfer systems are much more complex; thus, disturbances and specimen-actuator interactions may also affect actuator control performance.

One way to cope with the aforementioned uncertainties in time delay, control performance, and prediction inaccuracy is based on an upper bound delay technique that will be presented in the next section. As stated by the terminology of upper bound or overcompensation, the assumed delay τ_c for a displacement prediction is deliberately assumed to be larger than the actual system delay τ. This differs from the usual delay compensation schemes where $\tau_c = \tau$. For clarity hereafter, we name the latter assumption as the conventional delay compensation technique.

3. DELAY OVERCOMPENSATION AND OPTIMAL FEEDBACK

The idea behind the new compensation technique is to assume an upper bound delay τ_c not less than the possible maximum delay present in the RHS and use it for prediction; then, the actual delay will be overcompensated. In greater detail, let the desired displacement be achieved earlier than it should be and then find the corresponding reaction force to be fed back to the NS. With reference to Figure 4, the procedure of the overcompensation scheme can be described as follows:

DOI: 10.1002/eqe

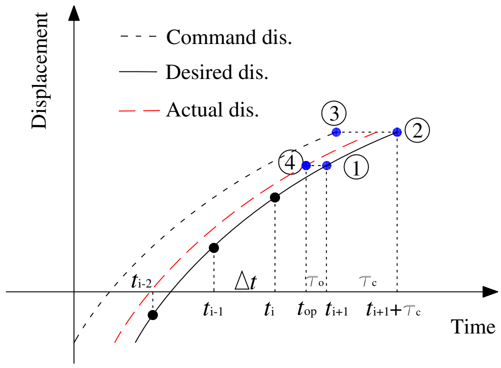

Figure 4. Schematics of the proposed overcompensation scheme.

(1) calculate the structural response x_{i+1};
(2) predict $x(t_{i+1}+\tau_c)'$, that is, the displacement at $t_{i+1}+\tau_c$, where τ_c is an upper bound system delay;
(3) send out the predicted displacement at t_{i+1};
(4) and search for the measured feedback force $r_m(t)$, corresponding to the closest measured displacement $x_m(t)$ to x_{i+1}, and feedback the force to the NS.

Evidently, as long as the chosen displacement in Step (4) above matches x_{i+1}, exact delay compensation is achieved, which means that the measured force $r_m(t)$ corresponds to the desired displacement x_{i+1} without errors owing to prediction methods and actuator control. Compared with conventional delay compensation methods, no matter how error exists in the predicted displacement, we minimize errors by choosing, from among recent data, the displacement $x_m(t)$ nearest to the desired one x_{i+1}. As a result, satisfactory properties such as error reduction and stability improvement can be expected.

At this stage, a key problem is how to optimally select the displacement measurement $x_m(t)$ and the corresponding feedback force $r_m(t)$. As shown schematically in Figure 4, the desired displacement is achieved τ_O ahead of the targeted time t_{i+1} because of overcompensation. However, we do not know the exact value of τ_O, and therefore, we need to seek τ_O in a certain time range so that the measured displacement at $t_{i+1}-\tau_O$ is as close as possible to x_{i+1}, and ideally equal to x_{i+1}. To ensure that τ_O can be found, we may assume τ_{0m} as the maximum τ_O and find out τ_O within the time range $[0, 2\tau_{0m}]$. In other words, the optimal problem can be described as follows: find $t_{op}=\{t\in[t_{i+1}-2\tau_{0m}, t_{i+1}]:\min|x_m(t)-x_{i+1}|\}$. Because $\tau_O=\tau_c-\tau$, τ_{0m} may be determined on the basis of the estimation of minimum of actual delay τ in the interested frequency range. If there are two optimal $x_m(t)$s, which may occur around the time when the displacement peaks, the one such that the corresponding velocity has the same sign as that associated with the desired displacement should be chosen. For the particular case shown in Figure 5, B' rather than B'' is chosen because the

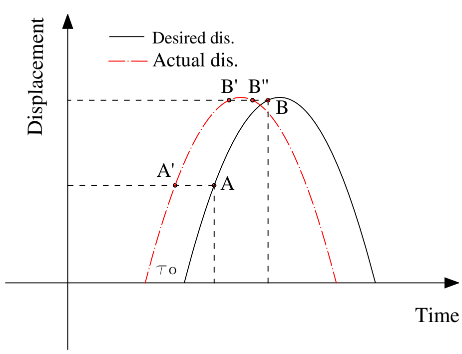

Figure 5. Overcompensation strategy in a particular case.

velocities of B' and B are both positive. In the optimization process, because the amount of data in the time range chosen is usually limited, the optimal $x_{\mathrm{m}}(t)$ can be determined simply by comparing all the data involved, and hence, no iteration is needed. For example, the amount of data will be 21, if the search range for τ_{O} is $[0,\ 2\Delta t]$, $\Delta t = 10/1024$ s, and sampling frequency of displacement measurement is 1024 Hz.

One of the important issues of the proposed compensation method is how to determine an appropriate upper bound delay. The upper bound can be estimated with the possible largest stiffness of specimen during the test, as the delay increase with increasing stiffness. For most civil engineering structures, they usually exhibit softening behavior. So the upper bound of delay may be determined on the basis of initial stiffness of the specimen. If, for some reason, the real delay is greater than the assumed upper bound, then the over-compensation retreats to conventional compensation with a fixed delay equal to the assumed upper bound, which is obviously still advantageous compared with the conventional compensation with a delay estimate less than the assumed upper bound.

Note that, for a specimen that is dependent on velocity, the optimal force feedback should be determined by searching the velocity response closest to the desired velocity, rather than the displacement response closest to the desired displacement. So the over-compensation is applicable to velocity-dependent specimens too. Of course, more challenges may arise when a specimen depends on both velocity and displacement. This is an open problem that deserves further studies not only for the compensation proposed in this paper but also for other compensation schemes.

4. NUMERICAL SIMULATIONS

4.1. Linear case

This section presents numerical simulations with the upper bound delay compensation presented in Section 3. Both second-order and third-order Hermite predictions described in Equations (6) and (7), respectively, for the SDOF system shown in Figure 2 are considered. For time integration, we use the LSRT2 method with a time integration interval $\Delta t = 0.01$ s. The mass of the structure model is set equal to 1 kg, while the stiffness $k_{\mathrm{n}} = k_{\mathrm{e}} = 200$ N/m is chosen such that $\Omega = 0.2$. The actual delay τ is assumed constant and equal to Δt. For conventional compensation, the compensated delay used in the prediction formula is equal to actual delay, that is, $\tau_{\mathrm{c}} = \tau$, whereas for the overcompensation scheme with an upper bound delay, $\tau_{\mathrm{c}} = 1.5\Delta t$.

For the LRST2 method combined with conventional compensation schemes, the calculated responses both at the intermediate step and at the end of the time step are used for prediction. However, the time instant corresponding to the response at the intermediate step, $y_{i+0.5}$, is not necessarily equal to $t_{i+0.5}$, and the LRST2 algorithm does not describe how to determine this time instant. For simplicity, it is assumed to be at the midpoint between t_i and t_{i+1}, that is, at $t_{i+0.5}$, on the basis of which stability analysis is carried out in the last section. Numerical simulations show, however, that this assumption may result in oscillation of displacement prediction and hence of the actuator command. To avoid command oscillation, we use the information at t_i instead of $t_{i+0.5}$, and the information at t_{i+1} as well, to predict the displacement response x'_{i+3} at t_{i+3}. Then, this predicted displacement is sent out to the actuator with a linear interpolation from $t_{i+0.5}$ to $t_{i+1.5}$. Apparently, this treatment leads to $0.5\Delta t$ of overcompensation. Hence, the optimal measured displacement can be sought in the time span Δt according to the procedure described in Section 3.

Figure 6 shows simulation results of free vibration with an initial displacement of 0.01 m, in which the second-order Hermite prediction is employed. Clearly, the conventional compensation entails algorithmic dissipation, in agreement with the spectral properties depicted in Figure 3. Conversely, the proposed delay overcompensation scheme effectively reduces dissipation and provides more accurate results, consistent with analysis in Section 3.

To further reveal the characteristics behind the favorable accuracy of overcompensation, the solutions of optimal displacement measurements are examined. In this respect, we define an indicator J, as the number of times in which the measured displacement is equal to the desired

DOI: 10.1002/eqe

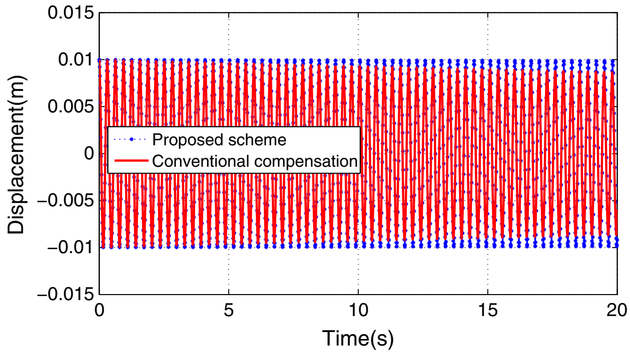

Figure 6. Numerical results provided by the second-order Hermite prediction.

displacement in each optimization process. Thus, $J=0$ indicates that no measured displacement is identical to the desired displacement, whereas $J=1$ and $J=2$ mean that one and two displacement measurements are identified equal to the desired displacement, respectively. The cases of $J=1$ and $J=2$ are illustrated in Figure 5. Among 4000 time integration points, with two points in each time step owing the two-stage LSRT2 method, there are 35, 3922, and 43 for $J=0,1,2$, respectively. In greater detail, $J>0$ indicates exact compensation, and hence, perfect compensation is achieved for 99.12% of the total simulation time. When the amplitude of the actual displacement is less than the desired one, J will be zero around displacement peaks.

Figure 7 shows the results provided by the third-order Hermite prediction. The conventional compensation brings an unstable response as expected by the spectral analysis shown in Figure 3, whereas the result of the overcompensation scheme accurately matches reference results. In this particular case, there are 32, 3875, and 93 in 4000 time integration points for $J=0,1,2$, respectively, again indicating perfect compensation for most of the time steps.

4.2. *Nonlinear case*

In this subsection, we consider a PS with a bilinear hysteretic force–displacement relationship. The yielding displacement and strain-hardening ratio of the specimen are 25 mm and 0.115, respectively. The initial stiffness of the specimen is 44.41 N/m, which is identical to the numerical stiffness and results in a frequency of the whole emulated structure equal to 1.5 Hz. The other parameters are the same as those employed in Section 4.1. The second-order Hermite prediction is employed for this nonlinear case. The El Centro earthquake (NS, 1940) with an acceleration peak 0.13 g is used.

The first 10 s of displacement time histories and force–displacement relationship of the PS are presented in Figures 8 and 9, respectively. For comparison, numerical results obtained by the central difference method and the time interval of 1 ms are presented as reference solution. The

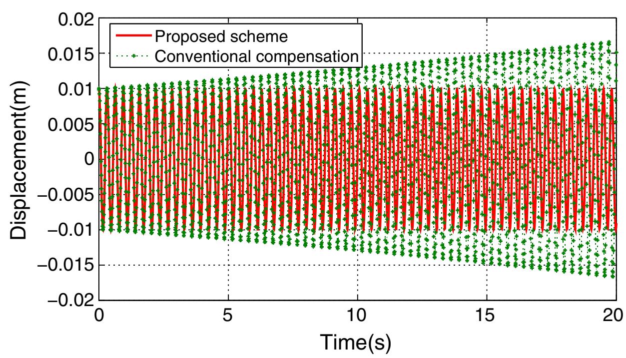

Figure 7. Numerical results provided by the third-order Hermite prediction.

DOI: 10.1002/eqe

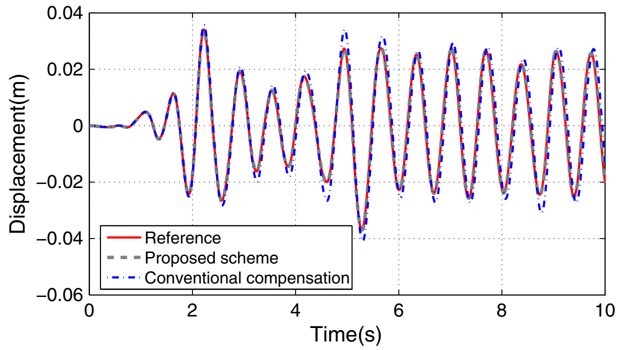

Figure 8. Displacement responses in the nonlinear regime provided by the overcompensation and conventional compensation schemes, compared with a reference solution.

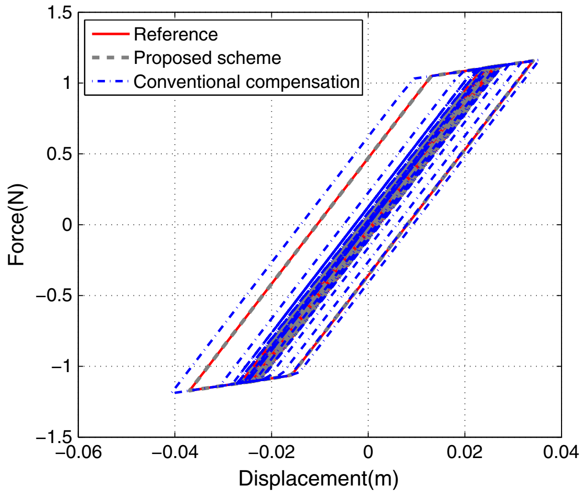

Figure 9. Force–displacement responses of the physical substructure.

displacement amplitude of the conventional compensation is larger than the reference solution. This result shows that the conventional compensation scheme based on the third-order prediction still results in some error although the hysteretic dissipation improves the response stability. Conversely, the displacement obtained with the overcompensation scheme matches the reference solution quite well. The indicator J is evaluated too and reads $J=0$, $J=1$, and $J=2$ for 45, 1946, and 9 time points, respectively. Like the linear case, exact compensation is achieved for most of the time. Note that in this nonlinear case, the restoring forces differ for the same optimal measured displacement for $J=2$, owing to the hysteretic force–displacement relationship. The force corresponding to the measured displacement with the same motion direction as desired is chosen as force feedback for response calculations.

It should be noted that actuators are modeled by means of a pure delay to simplify the spectral analysis in Section 2, and the pure delay model is also used in this section for numerical validation. The dynamics of an actuator system is in general dependent on both frequency and amplitude, and this behavior can generally be represented by a first-order transfer function. However, the uniqueness of the compensation presented in this paper is its robustness on delay variation, one source of which is the variation of input frequency. It has been validated by the numerical studies aforementioned and is to be further validated by the experimental studies in the next section. In addition, extra numerical analyses have shown that the proposed compensation technique offers even better results with a first-order model of actuator than with a pure delay model; hence, the pure delay model results in a conservative evaluation of advantage of the over-compensation scheme.

DOI: 10.1002/eqe

5. TEST VALIDATION

To check the performance of the delay compensation technique, some RHSs involving both SDOF and MDOF systems will be considered in this section.

5.1. Test setup

A versatile test system was conceived and installed at the University of Trento, Italy, to examine actuator control techniques and assess the reliability of RHS for linear/nonlinear MDOF structures. Basically, the system consists of four electromagnetic actuators and a dSpace DS1103 control board. The test rig design is flexible so that PS made up of springs, dampers, and masses with different mechanical properties can be configured as shown schematically in Figure 10. For the RHS considered here, the actuators were operated with a Proportional-Integral-Derivative (PID) controller tuned with the Chien, Hrones, and Reswick scheme for zero overshoot step response [20]. In addition, electromagnetic noise was reduced by an elliptic filter [21] with a pass frequency and a stop frequency of 20 and 30 Hz, respectively. The sampling frequency of both control and measurements were set equal to 1024 Hz.

5.2. Assessment of compensation accuracy with a prescribed displacement command

This subsection investigates the accuracy of the conventional and proposed compensation strategies with the aforementioned test system subject to a prescribed displacement command. Firstly, to evaluate the system delay, a test was performed with a sinusoidal command—in mm—which reads

$$x_c(t) = 10\sin(2\pi t). \tag{10}$$

To estimate the delay, the least square method is employed and formulated as

$$\min_{\tau} \frac{1}{n} \sum_{i=1}^{n} |x_c(t_i) - x_m(t_i - \tau)|^2. \tag{11}$$

In Equation (11), $x_m(\bullet)$ denotes the measured displacement, and n is the total number of data points. In the test, the time duration was 25 s, the sampling frequency 1024 Hz, and hence, $n = 25\,600$. The solution showed that the delay τ of the system was about 16.6 ms.

To investigate the effects of delay compensation, the actuator was commanded to realize a desired displacement containing three frequency components, expressed as

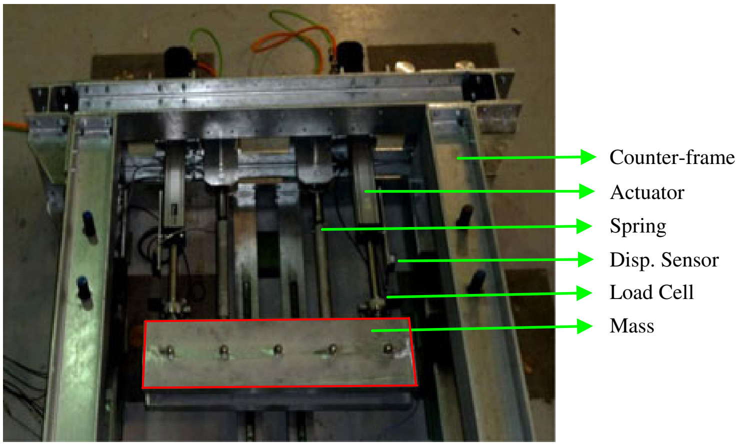

Figure 10. Photograph of test rig.

DOI: 10.1002/eqe

$$x(t) = 5\sin(2\pi t) + 3\sin(4\pi t) + 2\sin(8\pi t). \tag{12}$$

For the overcompensation strategy, the assumed upper bound delay τ_c was 20 ms for all RHSs, indicating that the delay was overcompensated by 3.4 ms. The optimal measured displacement was searched for in data of the last 12 ms. The third-order Hermite scheme was used for displacement prediction both in this and the next subsections. The proposed over-compensation scheme was compared with the conventional compensation scheme by means of the displacement errors defined as the actual minus the desired displacement, as depicted in Figure 11. By means of the overcompensation strategy, the standard deviation of error was reduced from 0.225 to 0.115 mm, nearly by half, while the peak error decreased slightly, that is, from 0.457 to 0.414 mm. Part of the desired, measured, and optimal displacements are shown in Figure 12, where we can see that the discrepancies between the desired and optimal displacements are small.

5.3. *RHS on an SDOF system endowed with a spring specimen*

The structure model is depicted in Figure 2, and relevant structural parameters are presented in Table I. The excitation is a sinusoidal load with a frequency of 1.3 Hz and amplitude of 300 N. The time step employed for the LSRT2 method is 10 ms. Three tests were carried out with a conventional

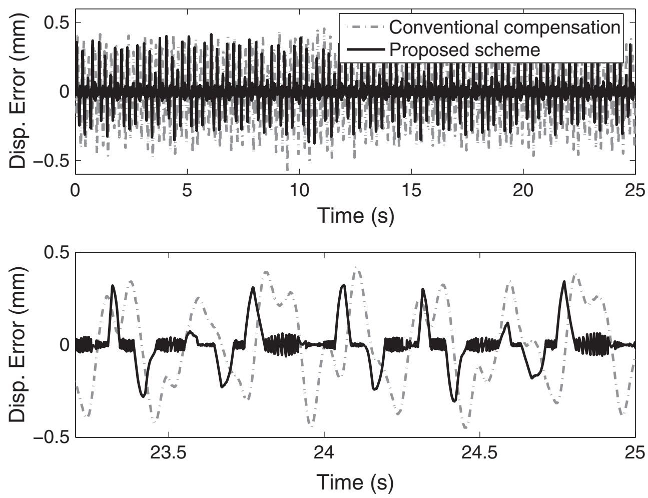

Figure 11. Global and close-up views of displacement errors in RHS with a sinusoidal command.

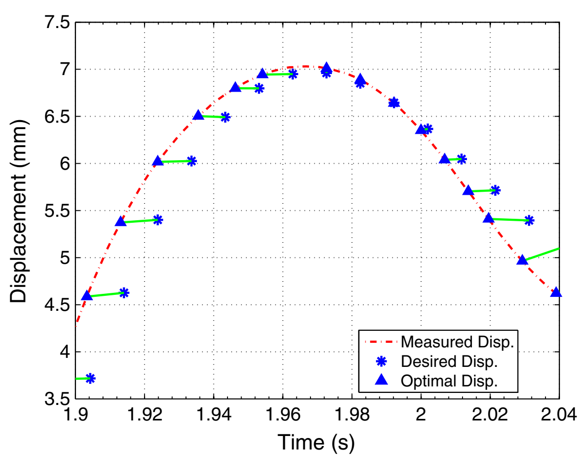

Figure 12. Desired, measured, and optimal displacements.

DOI: 10.1002/eqe

Table I. Structural parameters of the SDOF system.

m_n (kg)	k_n (kN/m)	c_n (kNs/m)	k_e (kN/m)	c_e (kNs/m)
1.52×10^3	20	0	40	0

compensation, an undercompensation with 15 ms, and the overcompensation method with an upper bound delay $\tau_c = 20$ ms. Figure 13 shows the displacement response of the RHS with overcompensation as well as the pure numerical result obtained by considering the friction force between the spring and the guide tube. The friction force was about 50 N, measured before the RHS. One can observe from Figure 13 that the response of the RHS matches the numerical simulation quite well. Figure 14 shows the displacement errors in the frequency domain for different compensation schemes. Clearly, the displacement error increased significantly even if the delay was underestimated by only 1.6 ms. In contrast, errors were remarkably reduced when the proposed overcompensation scheme was applied.

5.4. *RHS on a five-DOF system with a physical mass*

The whole structure consisted of a NS with five DOFs and a PS with an SDOF. The structure model is schematically depicted in Figure 15, where $k_0 = 200$ kN/m, $m_0 = 900$ kg, $k_{n1} = 160$ kN/m, $m_{n1} = 600$ kg, $k_e \approx 40$ kN/m, and $m_e \approx 298$ kg. The natural frequencies of the five modes were 0.68, 1.97, 3.11, 3.99, and 4.55 Hz, respectively. A sinusoidal force with amplitude 1 kN and frequency 1.5 Hz was imposed

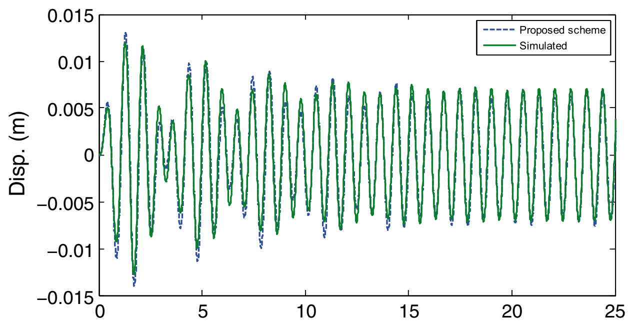

Figure 13. Comparison of RHS and numerical responses for an SDOF system.

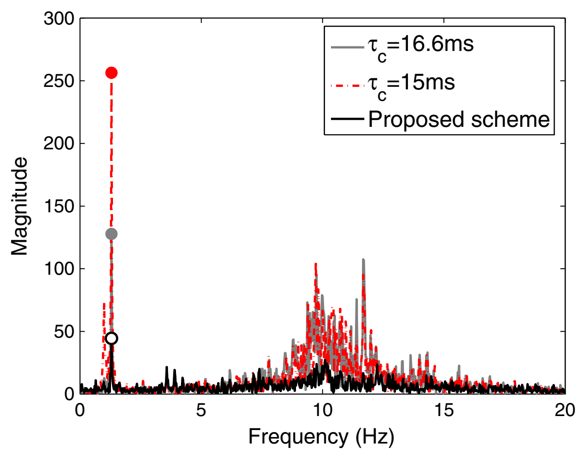

Figure 14. Displacement errors for RHS in the frequency domain.

DOI: 10.1002/eqe

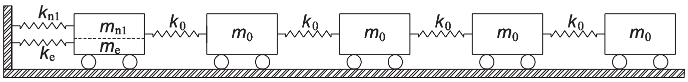

Figure 15. Computation model for the five-DOF system.

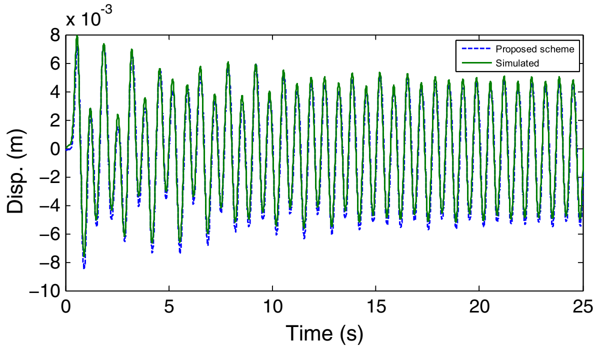

Figure 16. Comparison between RHS and numerical displacements for the physical substructure of the five-DOF system.

on the DOF to the right end in Figure 15. The second-order Hermite prediction was used for the compensation schemes. Both the displacement response from the RHS with overcompensation and the numerical result are presented in Figure 16. They basically agree well. The standard deviations of displacement errors were 0.169 and 0.0821 mm for conventional and overcompensation scheme, respectively, which reconfirms the effectiveness of the proposed method in terms of error reduction.

6. CONCLUSIONS

In this paper, a new scheme for delay compensation consisting of an upper bound delay and optimal feedback is proposed. The main conclusions are summarized here.

(1) The stability of RHS with time delay is related not only to compensation methods but also to concurrent integration methods. Even when time delay is exactly known, with conventional compensation methods, some combinations of numerical integration schemes and displacement prediction techniques may reduce response stability and lead to unconditional instability in the worst cases.
(2) A nearly exact delay compensation scheme is proposed, in which the displacement is overcompensated by means of an upper bound delay, and then, the datum closest to the desired displacement is picked out by an optimal process. The advantages of this scheme over conventional compensations for delay have been shown both through numerical simulation and by actual hybrid simulation.

Work is in progress to verify the effectiveness of the proposed compensation scheme based on an upper bound delay when several PSs are involved.

APPENDIX A: Stability of the explicit Newmark integration scheme with a linear acceleration prediction

For an RHS, the equation of motion of an undamped linear SDOF system discretized with the explicit Newmark method reads as follows:

$$m_n \ddot{x}_{i+1} + k_n x_{i+1} + r_{e,i+1} = f_{i+1} \tag{A.1}$$

DOI: 10.1002/eqe

$$x_{i+1} = x_i + \Delta t \dot{x}_i + \frac{1}{2}\Delta t^2 \ddot{x}_i \tag{A.2}$$

$$\dot{x}_{i+1} = \dot{x}_i + \frac{1}{2}\Delta t(\ddot{x}_i + \ddot{x}_{i+1}). \tag{A.3}$$

To compensate for a delay τ, through a linearly varying acceleration [6, 8], the predicted displacement reads

$$x(t_{i+1}+\tau)' = x_i + (\Delta t+\tau)\dot{x}_i + \frac{1}{3}(\Delta t+\tau)^2\ddot{x}_i + \frac{1}{6}(\Delta t+\tau)^2\ddot{x}' \tag{A.4}$$

with

$$\ddot{x}(t_{i+1}+\tau)' = \ddot{x}_i + \frac{\Delta t+\tau}{\Delta t}(\ddot{x}_i - \ddot{x}_{i-1}) = (2+\eta)\ddot{x}_i - (1+\eta)\ddot{x}_{i-1}. \tag{A.5}$$

The value of x'_{i+1} can be calculated assuming $\tau = \Delta t$ and replacing $i+1$ with i in Equations (A.4) and (A.5). Then, the restoring force of a PS consisting of a linear spring can be obtained with

$$r_{e,i+1} = k_e x'_{i+1} \tag{A.6}$$

As a result and with the assumption $k_e = k_n$ we obtain the following amplification matrix $\mathbf{A}$:

$$\mathbf{A} = \begin{bmatrix} 1 & 1 & 1/2 & 0 & 0 \\ -\Omega^2/4 & 1-\Omega^2/4 & 1/2-\Omega^2/8 & 0 & -\Omega^2/4 \\ -\Omega^2/2 & -\Omega^2/2 & -\Omega^2/4 & 0 & -\Omega^2/2 \\ 0 & 0 & 1 & 0 & 0 \\ 1 & 2 & 10/3 & -4/3 & 0 \end{bmatrix} \tag{A.7}$$

and the corresponding state vector $\mathbf{X}_i = \left[x_i \quad \Delta t\dot{x}_i \quad \Delta t^2\ddot{x}_i \quad \Delta t^2\ddot{x}_{i-1} \quad x'_{i+1}\right]^T$. The relevant spectral radius is shown in Figure A1. At first glance, the stability limit Ω seems to be $\Omega = 0.82$; however, a careful reader can find that the spectral radius is greater than unity also for Ω close to zero. This can be rigorously proved by the Routh's stability criterion.

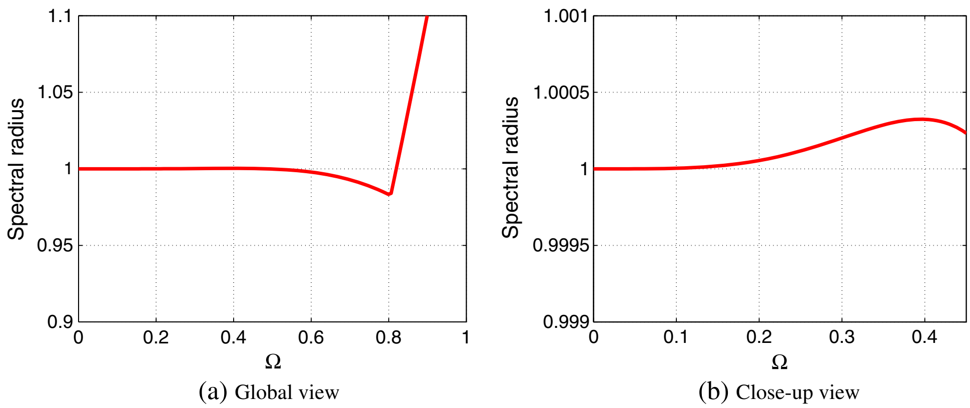

Figure A1. Spectral radius of the explicit Newmark integration scheme with a linear acceleration prediction.

DOI: 10.1002/eqe

In greater detail, the Routh's criterion is a well-known analysis tool for system stability in control theory. To apply this criterion, the characteristic polynomial associated with the time integrator is firstly expressed in terms of the complex s variable by replacing the eigenvalue variable λ with $(1+s)/(1-s)$. This process maps the unit circle characterized by $|\lambda|=1$, into the imaginary axis of the s-plane and the interior part of the circle into the left half of the s-plane [22]. As a result, the characteristic equation related to the amplification matrix (A.7) reads

$$6\lambda^5 + \left(-12 + 3\Omega^2\right)\lambda^4 + \left(13\Omega^2 + 6\right)\lambda^3 - 21\Omega^2\lambda^2 + 15\Omega^2\lambda - 4\Omega^2 = 0 \tag{A.8}$$

Substituting $\lambda=(1+s)/(1-s)$ into (A.8) yields

$$\left(12 + 25\Omega^2\right)s^5 + \left(36 - 41\Omega^2\right)s^4 + \left(36 - 2\Omega^2\right)s^3 + \left(12 + 6\Omega^2\right)s^2 + 9\Omega^2 s + 3\Omega^2 = 0 \tag{A.9}$$

Then, the array associated with the Routh criterion is obtained and tabulated in Table AI, with

$$\begin{array}{lll} b_1 = \dfrac{a_4a_3 - a_2a_5}{a_4} & b_2 = \dfrac{a_4a_1 - a_0a_5}{a_4} & c_1 = \dfrac{b_1a_2 - b_2a_4}{b_1} \\ c_2 = b_1 & d_1 = \dfrac{c_1b_2 - c_2b_1}{c_1} & e_1 = c_2 \end{array}. \tag{A.10}$$

Here, $a_i (i=0,1,2,\ldots,5)$ is the coefficient of the ith-order term in Equation (A.9). In addition, d_1 is expressed as

$$d_1 = \frac{64\left(262\Omega^4 - 183\Omega^2 + 18\right)\Omega^4}{1551\Omega^6 - 1288\Omega^4 + 2208\Omega^2 - 1152}. \tag{A.11}$$

It can be easily shown that, for small Ω, the elements of the first column of Table AI are all positive except d_1 that is negative. By the Routh criterion, Equation (A.9) contains roots with positive real parts, and the corresponding spectral radius of A is greater than one. This is consistent with what we observed from Figure A1(b).

The result of this analysis highlights a serious stability problem, when one tries to increase the algorithm accuracy by reducing the time step. Even worse, the combination of the explicit Newmark scheme with the linear acceleration prediction does not satisfy the zero-stability condition, which will be proved as follows.

The zero-stability concept regards the stability of an integrator when $\Delta t \to 0$, which is a necessary condition of convergence of a time integrator [23]. Let $\Delta t=0$ in Equation (A.7), and as a result, we have

Table AI. The array associated with the Routh's criterion.

a_5	a_3	a_1
a_4	a_2	a_0
b_1	b_2	0
c_1	c_2	0
d_1	0	
e_1		

DOI: 10.1002/eqe

$$\mathbf{A} = \begin{bmatrix} 1 & 1 & 1/2 & 0 & 0 \\ 0 & 1 & 1/2 & 0 & 0 \\ 0 & 0 & 0 & 0 & 0 \\ 0 & 0 & 1 & 0 & 0 \\ 1 & 2 & 10/3 & -4/3 & 0 \end{bmatrix}. \tag{A.12}$$

This matrix has eigenvalues $\lambda_{1,2}=1$ and $\lambda_{3,4,5}=0$. The eigenvalues of multiplicity two are apparently equal to one, and the corresponding eigenvectors can be easily shown to be linearly dependent. Therefore, $\mathbf{A}$ is unstable according to [22], and hence, the time integration method is not zero-stable.

APPENDIX B: Stability of the LRST2 method with a third-order Hermite polynomial prediction

We have shown in Figure 3 that the LRST2 method with the third-order Hermite polynomial prediction appears to be unconditionally unstable, which means that the spectral radius is greater than one for Ω close to zero. We prove this statement here with the techniques employed in Appendix 1.

The amplification matrix $\mathbf{A}$ is 6×6 and is characterized by a zero eigenvalue. Thus, the characteristic equation reduces to a fifth order and reads

$$\begin{aligned}&(4\gamma^4\Omega^4+8\gamma^2\Omega^2+4)\lambda^5+(-8\gamma^4\Omega^4+12\gamma^3\Omega^4-5/2\Omega^4\gamma^2+2\Omega^2-16\gamma^2\Omega^2-8)\lambda^4\\&\quad+(219/2\Omega^4\gamma^2-36\gamma^3\Omega^4+4\gamma^4\Omega^4-30\Omega^4\gamma+8\gamma^2\Omega^2+1/4\Omega^4+84\Omega^2\gamma-18\Omega^2+4)\lambda^3\\&\quad+(-54\Omega^4+52\gamma^3\Omega^4+42\Omega^2+324\Omega^4\gamma-168\Omega^2\gamma-987/2\Omega^4\gamma^2)\lambda^2\\&\quad+(-28\gamma^3\Omega^4+1589/2\Omega^4\gamma^2-22\Omega^2+84\Omega^2\gamma+201/4\Omega^4-392\Omega^4\gamma)\lambda\\&\quad+202\Omega^4\gamma-392\Omega^4\gamma^2-53/2\Omega^4=0\end{aligned} \tag{A.13}$$

The Routh criterion yields the same array as that shown in Table AI, but its elements are determined by Equation (A.13). In this particular case, the coefficient d_1 has the form

$$d_1=\frac{nun(\Omega)}{den(\Omega)}\Omega^4 \tag{A.14}$$

where *num* and *den* are two polynomials that depend on Ω. In addition, as $\Delta t\rightarrow 0$, $d_1/\Omega^4\rightarrow 128\gamma^3+496\gamma^2-656\gamma+136$; moreover, if $\gamma=1-\sqrt{2}/2$, $128\gamma^3+496\gamma^2-656\gamma+136\approx-10.37<0$, whereas the other five elements in the first column are all positive for small Ω. Therefore, the method is not stable when Ω is small. This result matches the trend observed from Figure 3.

The zero-stability analysis can be performed here as before. Therefore, for $\Delta t=0$, we have

$$\mathbf{A} = \begin{bmatrix} 1 & 1 & 0 & 0 & 0 & 0 \\ 0 & 1 & 0 & 0 & 0 & 0 \\ 1 & 3/2 & 0 & 0 & 0 & 0 \\ 0 & 0 & 0 & 0 & 1 & 0 \\ 0 & 0 & 0 & 0 & 0 & 1 \\ 1 & 2 & 0 & 0 & 0 & 0 \end{bmatrix}. \tag{A.15}$$

Again, we find that $\lambda_{1,2}=1$ and hence also this method is not zero stable according to [22].

ACKNOWLEDGEMENTS

The authors gratefully acknowledge the financial support of the National Science Foundation of China (grant numbers: 51161120360 and 90715036), the Fundamental Research Funds for the Central Universities (grant numbers: HIT. BRET2.2010009, HIT.ICRST2010016), and the European Union through the SERIES project (grant number: 227887).

REFERENCES

1. Nakashima M, Kato H, Takaoka E. Development of real-time pseudo dynamic testing. *Earthquake Engineering and Structural Dynamics* 1992; **21**(1):79–92.
2. Saouma V, Sivaselvan M (eds). *Hybrid Simulation: Theory, Implementation and Applications*. Taylor & Francis: London, 2008.
3. Bursi OS, Wagg D (eds). *Modern Testing Techniques for Structural Systems: Dynamics and Control*. Springer Wien: New York, 2008.
4. Wu B, Deng L, Yang X. Stability of central difference method for dynamic real-time substructure testing. *Earthquake Engineering and Structural Dynamics* 2009; **38**(14):1649–1663.
5. Bursi OS, Gonzalez-Buelga A, Vulcan L, Neild SA, Wagg DJ. Novel coupling Rosenbrock-based algorithms for real-time dynamic substructure testing. *Earthquake Engineering and Structural Dynamics* 2008; **37**(3):339–360.
6. Horiuchi T, Konno T. A new method for compensating actuator delay in real-time hybrid experiments. *Philosophical Transactions of the Royal Society of London, Series A: Mathematical, Physical and Engineering Sciences* 2001; **359**(1786):1893–1909.
7. Burden RL, Faires JD. *Numerical Analysis* (Ninth edn). Brooks Cole Cengage Learning: Canada, 2010.
8. Ahmadizadeh M, Mosqueda G, Reinhorn AM. Compensation of actuator delay and dynamics for real-time hybrid structural simulation. *Earthquake Engineering and Structural Dynamics* 2008; **37**(1):21–42.
9. Jung RY, Shing PB, Stauffer E, Thoen B. Performance of a real-time pseudodynamic test system considering nonlinear structural response. *Earthquake Engineering and Structural Dynamics* 2007; **36**(12):1785–1809.
10. Carrion JE, Spencer BF. Model-based strategies for real-time hybrid testing. *NSEL Report No.NSEL-006*. Department of Civil and Environmental Engineering, University of Illinois at Urbana-Champaign, 2007.
11. Chen C, Ricles J. Improving the inverse compensation method for real-time hybrid simulation through a dual compensation scheme. *Earthquake Engineering and Structural Dynamics* 2009; **38**(10):1237–1255.
12. Christenson R, Lin Y, Emmons A, Bass B. Large-scale experimental verification of semiactive control through real-time hybrid simulation. *Journal of Structural Engineering* 2008; **134**(4):522–534.
13. Darby AP, Williams MS, Blakeborough A. Stability and delay compensation for real-time substructure testing. *Journal of Engineering Mechanics* 2002; **128**(12):1276–1284.
14. Wallace MI, Wagg DJ, Neild SA. An adaptive polynomial based forward prediction algorithm for multi-actuator real-time dynamic substructuring. *Proceedings of the Royal Society A: Mathematical, Physical and Engineering Science* 2005; **461**(2064):3807–3826.
15. Chen C, Ricles J. Tracking error-based servohydraulic actuator adaptive compensation for real-time hybrid simulation. *Journal of Structural Engineering* 2010; **136**(4):432–440.
16. Wallace MI, Sieber J, Neild SA, Wagg DJ, Krauskopf B. Stability analysis of real-time dynamic substructuring using delay differential equation models. *Earthquake Engineering and Structural Dynamics* 2005; **34**(15):1817–1832.
17. Horiuchi T, Inoue M, Konno T, Namita Y. Real-time hybrid experimental system with actuator delay compensation and its application to a piping system with energy absorber. *Earthquake Engineering and Structural Dynamics* 1999; **28**(10):1121–1141.
18. Nakashima M, Masaoka N. Real-time on-line test for MDOF systems. *Earthquake Engineering and Structural Dynamics* 1999; **28**(4):393–420.
19. Wu B, Xu G, Wang Q, Williams MS. Operator-splitting method for real-time substructure testing. *Earthquake Engineering and Structural Dynamics* 2006; **35**(3):293–314.
20. Åström KJ, Hägglund T. *PID Controllers: Theory, Design, and Tuning* (2nd edn). Instrument Society of America: Research Triangle Park, N.C., 1995.
21. Mitra SK. *Digital Signal Processing: a Computer-Based Approach* (2nd edn). McGraw-Hill Companies, Inc: Tsinghua University Press, Beijing, China, 2001.
22. Hughes T. Analysis of transient algorithms with particular reference to stability behavior. *Computational Methods for Transient Analysis*, Belytschko T, Hughes TJR (eds). North Holland: Amsterdam, 1983.
23. Stuart A, Humphries AR. *Dynamical Systems and Numerical Analysis*. Cambridge University Press: New York, 1998.

DOI: 10.1002/eqe